04

Correlation restoration of images by nonlinear superimposed Fourier holograms

© A.V. Pavlov

ITMO University, St. Petersburg, Russia

e-mail: avpavlov@itmo.ru, aleksandrv.pavlov@yandex.ru

Received December 06, 2024
Revised January 27, 2025
Accepted January 31, 2025

The responses of sub-holograms self-formed as part of a multiplex hologram when recording superimposed holograms forming it in a $4f$ Fourier holography scheme with angular multiplexing of plane reference waves on a recording medium with quadratic nonlinearity of the exposure characteristic are considered. The sub-holograms implement a model of correlation restoration of the images described by the complex-valued amplitudes hetero-associative memory. The model can be related to the concept of Ghost Imaging: the response of each sub-hologram is described by convolution of the reference image used to record a superimposed hologram with the function of correlation of the input field with the reference image of another superimposed hologram. The inversion by the sub-holograms of the specific weights of the reference images in the responses relative to their ratio when recording the superimposed holograms is shown. An analysis of the correlation mechanism of amplification in the response of the amplitude of the restored reference image under its size decreasing in relative to the constant size of another reference image is given. The theoretical conclusions are confirmed by numerical simulation.

Keywords: Holography, Superimposed Holograms, Fourier-transform, Correlation, Restoration, Non-linear Exposure Characteristic, Ghost Imaging.

DOI: 10.61011/EOS.2025.04.61412.7424-24

Introduction

The progress of holography is inextricably linked to the implementation of correlation models of data processing; of note here are holographic correlators [1], associative memory based on them [2], and regression models [3]. A significant number of current studies in the field of optoinformatics are focused on the so-called „ghost" models and methods. Research in this direction, which relies on mutual correlation of two wave fields, was initiated in quantum optics [4–6] in experiments with pairs of correlated photons generated during spontaneous parametric down-conversion [7] and then extended to classical optics of fields and sources with thermal statistics [8–11]. It covers a wide range of current problems in image transmission and restoration (ghost imaging) [8–14]: endoscopy of three-dimensional spatially transparent objects [12,13] with the use of spatiotemporal correlations [14], polarimetry [15,16], remote sensing [17], cryptography [18–20], microscopy [21,22], etc.

The practical appeal of ghost methods often lies in the possibility of using an integrating sensor instead of an imaging one at the first stage (recording of the original image) [12–14]. However, since ghost models are based on correlation (quantum or classical), one has to pay the price of high computational costs at the image restoration stage to compensate for instrumental gain at the imaging stage. Therefore, methods of operational calculus with natural parallel processing of two-dimensional data arrays, of which holography is an example, are relevant here [1–3]. In addition, conceptually important is the analogy in the presence of two data (images, fields, beams) arrays in both ghost models and holography: a reference array and a signal one. It should be stressed here that classical ghost optics operates with intensity correlation, while holography deals with correlation of fields of complex amplitudes. The latter aspect is what makes holography relevant in phase contrast imaging, which is common in biological and medical research [12–14,21,22].

One may tentatively distinguish two scenarios of application of holography in ghost models: (a) its use for introduction of phase masks, which are needed to obtain the required amplitude field in the plane of the studied object in computational ghost imaging [16,20], into the circuit by means of space-time light modulators; (b) ghost holography [21,22]. In the latter case, the optical circuit is complicated by the addition of a third random field, which acts as a reference field for hologram recording, to two beams of the ghost diffraction arrangement (signal and reference ones) [21]. However, these implementations do not solve the topical problem of computational complexity, since they include stages of conventional digital calculations [22].

The application of holographic methods within correlation models is largely based on linear recording of holograms. However, the exposure characteristics (ECs) of holographic recording media (HRM) are nonlinear. Important in this context is the study of V.V. Orlov [23], who has demonstrated theoretically that when superimposed holograms are recorded with angular multiplexing of reference beams on an HRM with quadratic nonlinearity of the EC, sub-holograms relating the wave fields recorded on

different superimposed holograms are formed in a multiplex hologram at the stage of its development. This result, which represents a special case of emergence of combination frequencies in a nonlinear system [24], was updated to the $4f$ Fourier holography scheme and verified experimentally in [25].

In furtherance of this approach, we demonstrate below that quadratic sub-holograms in a multiplex Fourier hologram implement the model of correlation image restoration that may be associated with the concept of ghost images. The mechanism of inversion of specific weights of patterns restored by sub-holograms relative to template ones is illustrated with a focus on the scenario of preference for various possible applications: constancy of the specific weight of the reference template at the stage of recording and reduction of the restored one.

1. Approach and model

1.1. Optical circuit

Figure 1 shows the classical $4f$ Fourier holography scheme with a multiplex hologram formed by two superimposed holograms recorded sequentially with spatial separation of point off-axis reference sources (angular multiplication of reference beams with a plane wave front). In what follows, the term „pattern“ denotes a field of complex amplitudes in the corresponding plane.

When superimposed holograms are recorded in the arrangement presented in Fig. 1, the following intensity distributions recorded sequentially on the HRM form in Fourier plane H (the rear focal plane of the first Fourier-transform lens L_1):

$$I_A(\nu_x, \nu_y) \propto \left[D^A \exp(j2\pi\nu_x x^A) + \Im(A(x,y))\right] \times \left[D^A \cdot \exp(j2\pi\nu_x x^A) + \Im(A(x,y))\right]^*,$$

$$I_B(\nu_x, \nu_y) \propto \left[D^B \exp(j2\pi\nu_x x^B) + \Im(B(x,y))\right] \times \left[D^B \cdot \exp(j2\pi\nu_x x^B) + \Im(B(x,y))\right]^*,$$

where ν is the spatial frequency, j is the imaginary unit, D^A and D^B are the real amplitudes of plane wave fronts proportional to the amplitudes of the corresponding point reference sources characterized by delta functions $\delta_A(x - x_A, y)$ and $\delta_B(x - x_B, y)$, x^A and x^B are their coordinates, and $\Im$ and an asterisk denote Fourier transform and complex conjugation, respectively.

If a latent image in the HRM is developed after the recording of all superimposed holograms and the nonlinear HRM EC may be approximated by the first two terms of its expansion in a power series, the dependence of local diffraction efficiency of the hologram in amplitude on spatial frequency takes the form

$$\begin{aligned} H(\nu_x, \nu_y) &= H^1(\nu_x, \nu_y) + H^2(\nu_x, \nu_y) \\ &= h^1 \Big\{ [D^A \cdot \exp(j2\pi\nu_x x^A) + \Im(A(x,y))] \\ &\quad \times [D^A \cdot \exp(j2\pi\nu_x x^A) + \Im(A(x,y))]^* \\ &\quad + [D^B \cdot \exp(j2\pi\nu_x x^B) + \Im(B(x,y))] \\ &\quad \times [D^B \cdot \exp(j2\pi\nu_x x^B) + \Im(B(x,y))]^* \Big\} \\ &\quad + h^2 \Big\{ [D^A \cdot \exp(j2\pi\nu_x x^A) + \Im(A(x,y))] \\ &\quad \times [D^A \cdot \exp(j2\pi\nu_x x^A) + \Im(A(x,y))]^* \\ &\quad + [D^B \cdot \exp(j2\pi\nu_x x^B) + \Im(B(x,y))] \\ &\quad \times [D^B \cdot \exp(j2\pi\nu_x x^B) + \Im(B(x,y))]^* \Big\}^2. \end{aligned} \tag{1}$$

where superscripts 1 and 2 denote linear and quadratic expansion terms and h^1 and h^2 are the coefficients depending on the EC and the conditions of HRM development. The expansion of the quadratic term in (1) (elementary but rather cumbersome calculations are omitted here) yields, among other things, two terms, each of which characterizes the interference of reference patterns $A(x, y)$ and $B(x, y)$ that do not interfere in reality:

$$H^{B2}(\nu_x \cdot \nu_y) = h^2 D^A D^B \Im^*(A(x,y)) \Im(B(x,y)) \times \exp(j2\pi\nu_x(x^A - x^B)), \tag{2.1}$$

$$H^{B2}(\nu_x \cdot \nu_y) = h^2 D^A D^B \Im(A(x,y)) \Im^* B(x,y) \times \exp(-j2\pi\nu_x(x^A - x^B)). \tag{2.2}$$

In what follows, we call these components of multiplex hologram (1) quadratic sub-holograms; for brevity, the definition „quadratic“ is also omitted by default.

When pattern $In(x, y)$ is presented in input plane P_1 of the circuit in Fig. 1, sub-holograms form two responses in output plane P_2 that are positioned symmetrically relative to the principal optical axis at distances $(x^A - x^B)$ and $-(x^A - x^B)$ from it:

$$\begin{aligned} B^R(\Delta_x, \Delta_y) &= h^2 D^A D^B \Im\left[\Im(In(x,y)) \Im^*(A(x,y)) \times \Im(B(x,y)) \exp(j2\pi\nu_x(x^A - x^B))\right] \\ &= h^2 D^A D^B \left\{B(x,y) * [In(x,y) \otimes A(x,y)] * \delta(x^A - x^B)\right\} \\ &\propto B(x,y) * [In(x,y) \otimes A(x,y)], \end{aligned} \tag{3.1}$$

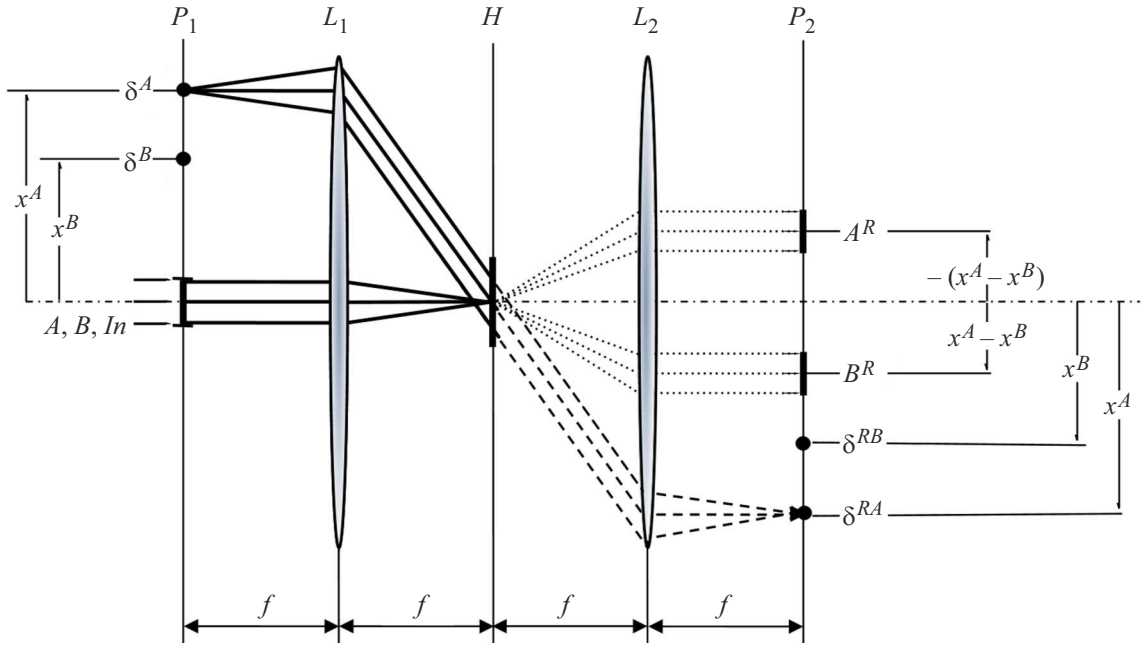

Figure 1. $4f$-Fourier holography scheme for two superimposed holograms: A, B, In — patterns: reference image ones and the input pattern, which are presented one after the other in input plane P_1 (short arrows represent the flat wave front illuminating the transparencies with patterns); δ^A and δ^B — point reference sources shifted by x^A and x^B relative to the principal optical axis, respectively; L_1, L_2 — the first and second Fourier-transform lenses with focal lengths f; H — Fourier hologram plane; and P_2 — response plane. Dashed lines trace the path of rays diffracted by superimposed hologram H^A and restoring the image of reference source δ^{RA} in plane P_2, while dotted lines trace the path of rays diffracted by quadratic sub-holograms H^{B2} and H^{A2}, which formed due to the quadratic nonlinearity of the HRM EC, and restoring patterns B^R and A^R, respectively.

$$
\begin{aligned}
A^R(\Delta_x, \Delta_y) &= h^2 D^A D^B \Im\big[\Im(In(x,y))\Im(A(x,y)) \\
&\times \Im^*(B(x,y))\exp(-j2\pi\nu_x(x^A - x^B))\big] \\
&= h^2 D^A D^B \left\{A(x,y) * [In(x,y) \otimes B(x,y)] * \delta(x^A - x^B)\right\} \\
&\propto A(x,y) * [In(x,y) \otimes B(x,y)],
\end{aligned}
\tag{3.2}
$$

where R in superscripts stands for „restored," Δ_x and Δ_y are the coordinates in plane P_2, and $*$ and $\otimes$ denote the convolution and correlation operations, respectively. Responses (3.1) and (3.2) of each of the quadratic sub-holograms (2.1) and (2.2) are essentially convolutions of one of the reference image with the correlation function of patterns (in square brackets): the input pattern and the other reference image, which, within this description, is defined formally (since reference image $A(x,y)$ and $B(x,y)$ do not interfere physically) as a reference. The reference image restored by a sub-hologram is also formally called a signal one. This distinction between signal and reference image is a matter of convention and is relevant only to a specific sub-hologram; the definitions for the second sub-hologram should be swapped.

1.2. Analysis of the model

Bulk HRM. Owing to the angular selectivity of a thick hologram, the correlation functions in (3.1) and (3.2) are reduced to the global maxima (GM) of the autocorrelation functions (ACFs) representing diffraction-limited images of point reference sources; their amplitudes are characterized by the scalar products of input and reference patterns: $\langle In(x,y)A(x,y)\rangle$ instead of correlation function $[In(x,y) \otimes A(x,y)]$ in (3.1) and $\langle In(x,y)B(x,y)\rangle$ instead of $[In(x,y) \otimes B(x,y)]$ in (3.2). Accordingly, the convolutions in (3.1) and (3.2) are reduced to the multiplication of reference images by these scalars

$$B^R(\Delta_x, \Delta_y) \propto B(x,y) \cdot \langle In(x,y)A(x,y)\rangle, \tag{4.1}$$

$$A^R(\Delta_x, \Delta_y) \propto A(x,y) \cdot \langle In(x,y)B(x,y)\rangle, \tag{4.2}$$

Thus, owing to the angular selectivity of a thick hologram, quadratic sub-holograms restore undistorted references, but with a loss of resolution due to additional filtering caused by the limited dynamic range and nonlinearity of the HRM EC [26,27].

Let us take the scalar product as a measure, introduce relation

$$k = \frac{\langle A(x,y)A(x,y)\rangle}{\langle B(x,y)B(x,y)\rangle},$$

and, taking (4.1) and (4.2) into account, determine the ratio of absolute amplitudes of reference image patterns (restored by the sub-holograms and the original ones) at the stage of

recording the superimposed holograms:

$$\frac{|B^R(x,y)|}{|B(x,y)|} \propto \langle In(x,y)A(x,y)\rangle = k\cdot\langle In(x,y)B(x,y)\rangle$$
$$= k\cdot\langle B(x,y)B(x,y)\rangle + k\langle\overline{B(x,y)}B(x,y)\rangle, \quad (5.1)$$
$$\frac{|A^R(x,y)|}{|A(x,y)|} \propto \langle In(x,y)B(x,y)\rangle = \frac{1}{k}\cdot\langle In(x,y)A(x,y)\rangle$$
$$= \frac{1}{k}\cdot\langle A(x,y)A(x,y)\rangle + \frac{1}{k}\langle\overline{A(x,y)}A(x,y)\rangle, \quad (5.2)$$

where $\overline{A(x,y)}$ and $\overline{B(x,y)}$ are the complements of each of the reference images to input field $In(x,y)$. It follows from (5.1) and (5.2) that if one of the reference images, e.g. $A(x,y)$

$$\langle A(x,y)A(x,y)\rangle > \langle B(x,y)B(x,y)\rangle,$$

was dominant in scalar product as a measure when superimposed holograms were recorded, the ratio of amplitudes of the restored patterns in responses of sub-holograms (3.1) and (3.2) is inverted relative to the reference image patterns: the amplitude of dominant reference image $A^R(x,y)$ restored by sub-hologram (2.2) is suppressed (5.2), while the amplitude of weaker pattern $B^R(x,y)$ in response (4.1) formed by sub-hologram (2.1) is, on the contrary, enhanced (5.1).

Thin HRM. The above analysis is also valid for a thin hologram. However, owing to its angular invariance, the restored patterns are characterized not by multiplication by a scalar (4.1) and (4.2), but by convolutions of reference images with full correlation functions, which include both the ACF GM and lateral maxima: auto- and cross-correlation functions represented by the second terms in (5.1) and (5.2). Owing to the internal correlation of the pattern, the ACF GM is not a delta function in the general case, but is characterized by a non-zero radius. Both these factors reduce the restored image quality: a non-zero correlation radius entails a loss of resolution, and lateral maxima form a background that is both superimposed on the restored reference image and surrounds it. To improve the quality of the restored pattern and increase its contrast against the background, one needs to maximize the signal-to-noise ratio (i.e., the ratio of the ACF GM amplitude to the average amplitude of lateral maxima of the correlation function) and reduce the correlation radius [28] (e.g., by means of spatial-frequency filtering [26,27] or by introducing orthogonalizing masks in input plane P_1 [29]).

Efficiency of separating the reference image from the back-ground. Let us introduce an estimate of efficiency of separating reference image $B^R(x,y)$ from background $\overline{B^R(x,y)}$ in restored field (4.1). This estimate characterizes the contrast (in amplitude) of the reference image against the background:

$$K^B = \frac{M|B^R(x,y)|}{M|\overline{B^R(x,y)}|}, \quad (6)$$

where $M|B^R(x,y)|$ is the absolute amplitude of the restored reference image averaged over its area and $M|\overline{B^R(x,y)}|$ is the area-average absolute background amplitude.

If the patterns may be characterized by realizations of a homogeneous isotropic centered random field,

$$\langle A(x,y)A(x,y)\rangle = \sigma^2 S^A, \quad (7)$$

where σ^2 is the field variance and S^A is the area of reference image $A(x,y)$ [28]. It follows from (7) that the dominance in scalar product is specified by two equivalent factors: variance σ^2 of the pattern (or its average absolute amplitude related to the variance) and its area S. The latter factor (i.e., the scenario where the reference images and input field $In(x,y)$ are essentially realizations of the same homogeneous isotropic random field) is the one of principal interest for, e.g., cryptography. It is evident from (7) that estimate K^B depends directly on area S^A of reference reference image $A(x,y)$ (but is not proportional to it due to the presence of cross-correlation components in (5.1)). The dependence (allowed by (5.1), but not characterized by (7)) of ratio (6) on area S^B of the signal reference image at constant S^A is less obvious. Its mechanism is examined below.

Let us present response (3.1) in the form

$$B^R(\Delta_x,\Delta_y) \propto B(x,y) * [A(x,y)\otimes A(x,y)]$$
$$+ B(x,y) * \left[\overline{A(x,y)}\otimes A(x,y)\right]. \quad (8)$$

The first term here characterizes two components:

(1.1) signal pattern restored by the ACF GM $B(x,y)$: $B(x,y) * \langle A(x,y)A(x,y)\rangle$;

(1.2) superimposed halo formed by the lateral ACF maxima $B(x,y) * [A(x,y)\otimes A(x,y)] - B(x,y) * \langle A(x,y)A(x,y)\rangle$.

(2) The second term in (8) characterizes the background, which is formed by the cross-correlation component, that surrounds $B^R(x,y)$ and is superimposed on it: $B(x,y) * [\overline{A(x,y)}\otimes A(x,y)]$.

To estimate the dependence of the average absolute amplitude of component (1.1) (restored signal reference image $B(x,y)$) on r, we characterize the dependence of the integral diffraction efficiency of sub-hologram H^{B2} on S^B as the dependence of the absolute amplitude of response in plane P_2 when the hologram is illuminated by a beam of unit amplitude with a plane wave front:

$$|Out^{B2}(\Delta_x,\Delta_y)| = |\Im(H^{B2}(\nu_x,\nu_y))|$$
$$\propto |B(x,y)\otimes A(x,y)| * \delta(x^A - x^B).$$

Since the reference images are assumed to be uncorrelated, the ensemble-average absolute response amplitude is the average amplitude of the cross-correlation field and, according to [28], the dependence of interest to us may be

estimated as follows:

$$\eta^B(S^B) \propto M|B(x,y) \otimes A(x,y)|$$
$$= \sqrt{\kappa S^B \sigma^4 S^{Corr}} \propto \sqrt{S^B} = \sqrt{\frac{S^A}{r}}, \qquad (9)$$

where M is the expectation symbol, κ is a coefficient depending on the field ACF type, σ^4 is its variance squared, S^{Corr} is the correlation area, and $r = \frac{S^A}{S^B}$ is the ratio of reference image areas.

With decreasing S^B, the following is the limiting case of existence of response $B(x,y) = \delta(x - x^B, y - y^B)$:

$$|Out^{B2}(\Delta_x, \Delta_y)| \propto |\delta(x - x^B, y - y^b) \otimes A(x,y)|$$
$$* \delta(x^A - x^B) = |A(x + (x^A - x^B), y)|,$$

therefore, the sought-for dependence of the average absolute amplitude of restored reference image $B(x,y)$ on its area or, equivalently, on ratio r of reference image areas (if area S^A of the reference reference image remains unchanged) takes the form

$$M^B(r) = M|B^R(x,y)| \propto \eta^B(r) \propto a + b \cdot r^{-0.5}, \qquad (10)$$

where a and b are parameters specified by the characteristics of reference images $A(x,y)$ and $B(x,y)$, respectively. We are interested not in the absolute values of diffraction efficiency, but only in its dependence on r; normalizing it to its value at $r = 1$, we obtain $a + b = 1$.

The contribution of component (1.2) is determined by the ratio of the GM and the lateral maxima of the ACF, which depends both on the ACF type, which specifies correlation area S^{Corr}, and on the ratio of areas of the reference reference image and the correlation $\Omega^A = \frac{S^A}{S^{Corr}}$, which is an information estimate of pattern $A(x,y)$ [28]. This factor has the above-discussed mechanism of dependence on S^B with one significant refinement: as was demonstrated in [26,28], the ratio of amplitudes of the GM and the lateral maxima of the ACF depends on the correlation area non-monotonically. As the area decreases, this ratio increases and, accordingly, the contribution of the component decreases, but when the correlation radius becomes approximately 2–3 times larger than the resolution element (pixel), the lateral maxima start to grow rapidly, reflecting the destruction of the internal correlation of the reference image and, accordingly, the enhancement of contribution of component (1.2) to the background component of the restored field.

To estimate the dependence of the average absolute amplitude of background $M|\overline{B^r(x,y)}|$ formed by the second term in (8) on r, we postulate that the area of background $\overline{A(x,y)}$ in the input pattern is no smaller than the area of reference reference image $A(x,y)$. When the average amplitude of cross-correlation field $\left|\overline{A(x,y)} \otimes A(x,y)\right|$ is estimated, reference reference image $A(x)$ then acts as a reference image, and, in accordance with [28], we find that the average amplitude of cross-correlation field $\left|\overline{A(x,y)} \otimes A(x,y)\right|$ does not depend on S^B or, equivalently, on the ratio of reference image areas r:

$$M\left|\overline{A(x,y)} \otimes A(x,y)\right| = \sqrt{\kappa S^A \sigma^4 S^{Corr}} \propto \sqrt{S^A}.$$

Applying the same approach [28] to the second term in (8) as a whole (i.e., considering the convolution as a correlation of $B(x,y)$ with $|\overline{A(x,y)} \otimes A(x,y)|$, which is valid within the adopted field model), we obtain the dependence of the area-averaged absolute amplitude of background $M|\overline{B^R(x,y)}|$ on the area of signal reference image S^B or the ratio of reference image areas r:

$$M^N(r) = M\left|B(x,y) * \left[\overline{A(x,y)} \otimes A(x,y)\right]\right|$$
$$= \sqrt{\kappa S^B \sigma^4 S^{Corr}} \propto \sqrt{S^B} \propto \frac{c}{r^{0.5}}, \qquad (11)$$

where c is a parameter.

Assuming that information measure Ω^A of the reference reference image is sufficiently high, we obtain an approximate dependence for the estimated efficiency of separating the reference image from the background by the introduced criterion of the ratio of the their average absolute amplitudes (contrast (6)):

$$K(r) = \frac{M^B(r)}{M^N(r)} \propto \frac{r^{0.5}}{c}(a + b \cdot r^{-0.5})$$
$$= \frac{1}{2}(a \cdot r^{0.5} + b) = \frac{1}{c}(1 + a(r^{0.5} - 1)). \qquad (12)$$

2. Numerical modeling

The responses of sub-holograms (2.1) and (2.2) were modeled for the thin HRM design, which is of greatest practical interest. A random centered field with a normal amplitude distribution within the $[-0.5, 0.5]$ interval was used as input pattern $In(x,y)$ (see the example in Fig. 2, *a*). The field variance was $\sigma^2 = 0.083$, and the correlation radius at the zero level was 1 pixel; i.e., the field was delta-correlated. The dimensions of input pattern $In(x,y)$ set the aperture size in input plane P_1 and were varied; the maximum size was 512×512 pixels ($S^{In} = 2.62144 \cdot 10^5$).

Non-overlapping fragments of the field were used as reference images $A(x,y)$ and $B(x,y)$. The areas of reference image $A(x,y)$ were $S^A = \frac{1}{16}S^{In}$ and $S^A = \frac{1}{4}S^{In}$, and the dimensions of reference image $B(x,y)$ were varied and set by the value of parameter $r = \frac{S^A}{S^B}$. For illustrative purposes, letters A and B were also used as reference images. Their outline was filled with field (Fig. 2, *b*), and the maximum area of the outline of the dominant reference image was $S^A = 2.613 \cdot 10^4 \approx 0.1 \cdot S^{In}$.

The dimension of sub-holograms was determined using the discrete Fourier transform as the dimension of the Fourier image of the aperture in input plane P_1. The geometric dimensions of the response field corresponded to the dimensions of the input aperture.

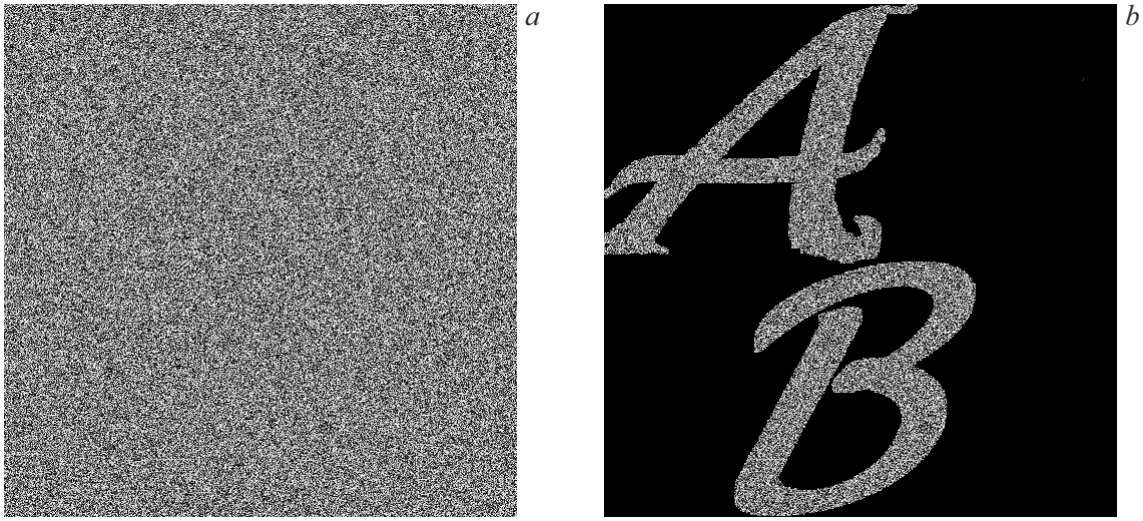

Figure 2. Examples of an input pattern containing both reference images $A(x, y)$ and $B(x, y)$: with background fill (a) and with just the $A(x, y)$ and $B(x, y)$ reference images filled (b).

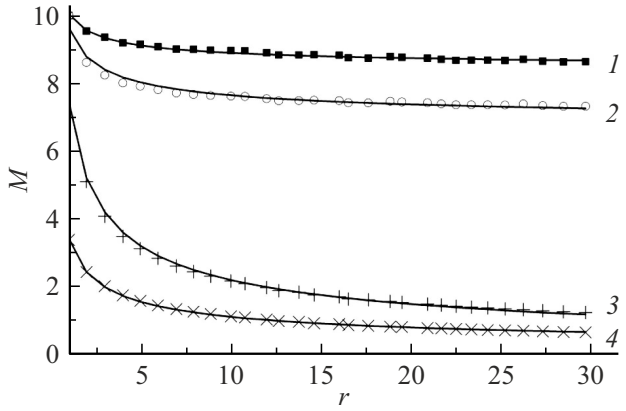

Figure 3. Dependences of the average absolute amplitude of the field fragments in Fig. 2, *a* restored by the quadratic sub-hologram (reference image pattern $B(x, y)$ (*1* and *2*) or the background (*3* and *4*)) on the ratio of reference image areas corresponding to the cases with only the reference reference image $A(x, y)$ (*1* and *3*) or the complete field $In(x, y)$ (*2* and *4*) presented in the input plane.

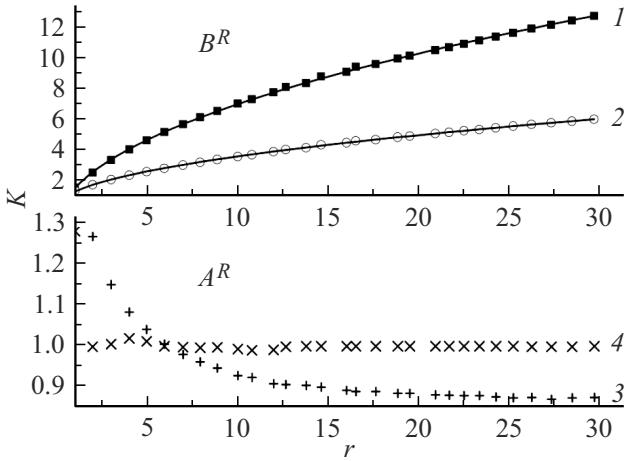

Figure 4. Dependences of the ratio of the average absolute amplitudes of the restored reference image and the background surrounding it on the ratio of reference image areas: *1* and *2* — for restored reference image pattern $B(x, y)$; *3* and *4* — for restored reference image pattern $A(x, y)$; with (*1* and *3*) only reference images $A(x, y)$ and $B(x, y)$ or (*2* and *4*) the complete $In(x, y)$ field (Fig. 2, *a*) presented in the input plane; points — measured values, curves — approximation (10): *1* — $K^B(r) = 2.502 \cdot r^{0.5} - 0.986$, $\delta K = 0.005$; *2* — $K^B(r) = 1.052 \cdot r^{0.5} + 0.206$, $\delta K = 0.004$.

It follows from (2.1) and (2.2) that sub-holograms record mutual shift $(x^{\mathrm{A}} - x^{\mathrm{B}})$ of the point reference sources rather than their absolute shifts x^{A} and x^{B}. According to (3.1) and (3.2), with a thin HRM, this shift is equivalent to the mutual displacement of reference images within the input aperture. The mutual shift of the reference images is exactly the parameter that was modeled (see Figs. 2, *b* and 5).

Figure 3 shows the dependences of the average absolute amplitudes of restored reference image $B(x, y)$ and the background normalized to the value of $M^B(1)$ for an input pattern 512×512 pixels in size and reference reference image $A(x, y)$ 256×256 present in it (Fig. 2, *a*) on the ratio of reference image areas r. The measured values were approximated by model (10).

The dependences for reference reference image $A(x, y)$ 128×128 and reference image letters were similar in nature (with the obvious difference that the spread of measured values relative to the approximating curve increased as the reference images grew smaller). The table lists the parameter values of model (10) and relative approximation errors δM^B for two reference image pattern sizes.

It is evident from the table that the values of parameter a for the input pattern with solid fill in Fig. 2, *a* (curves *3*

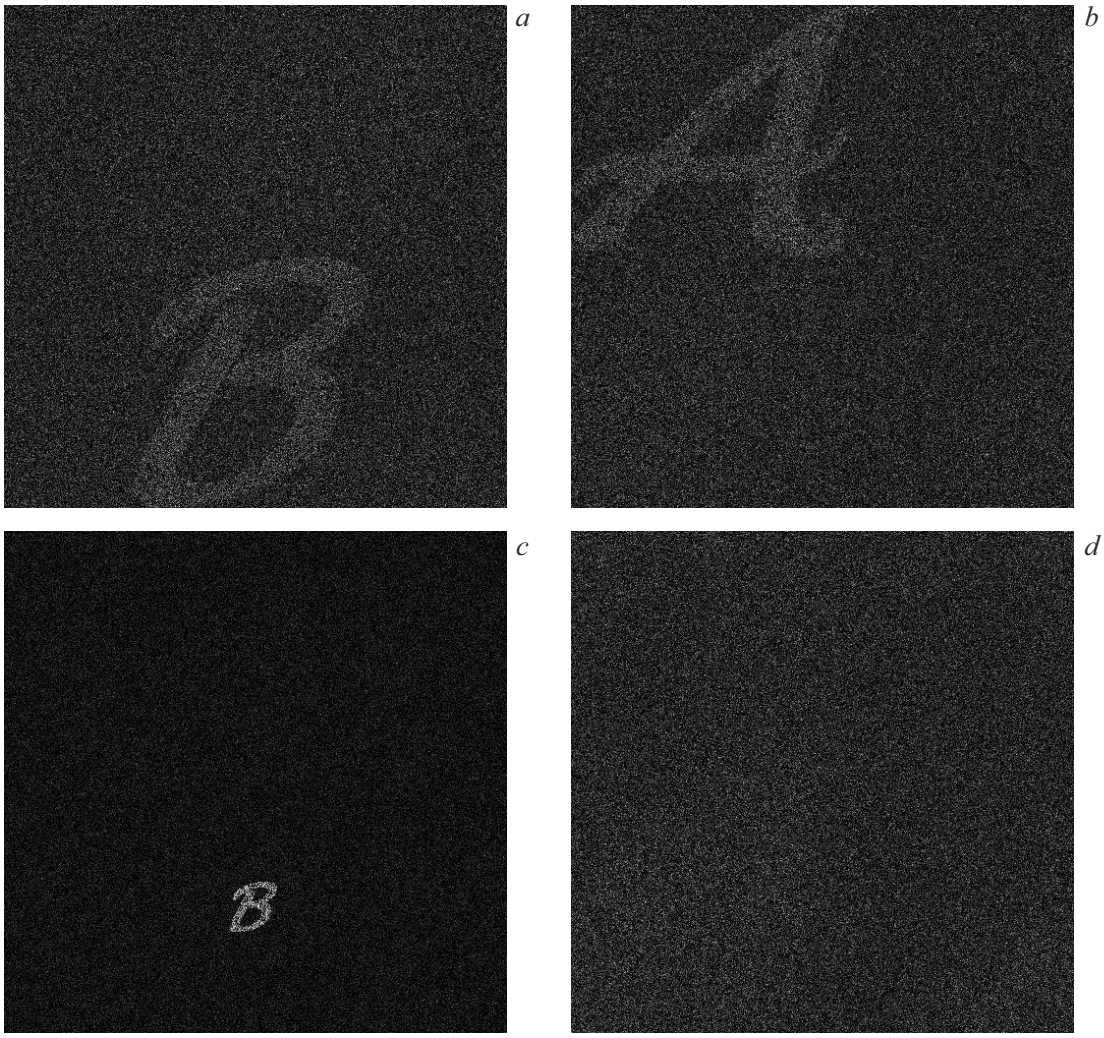

Figure 5. Sub-hologram responses: H^{B2} — left panels (a and c) and H^{A2} — right panels (b and d) for reference image area ratios $r = 1$ — top row and $r = 31$ — bottom row.

Parameter values and relative errors of approximation of the experimental data in Fig. 3 by model $M^B(r) = a + b \cdot r^{0.5}$ (10)

Parameter	Size (pix)	№ of the curve in Fig. 3			
		1	2	3	4
a	256×256	0.837	0.683	0.004	−0.023
	128×128	0.845	0.655	—	−0.014
b	256×256	0.167	0.29	0.337	0.766
	128×128	0.164	0.324	—	0.709
Error	256×256	0.003	0.009	0.011	0.024
δM^B	128×128	0.006	0.007	—	0.015

and *4*) are within the relative approximation error; i.e., one may be neglect them and use the approximate model of background amplitude (11).

Figure 4 shows the dependences of the estimated efficiency of separating a reference image from the background (ratio (6) of average absolute amplitudes of the restored reference images and the background) on ratio r of the reference image areas for an input pattern 512×512 pixels in size with a constant size of reference reference image $A(x, y)$ $S^A = 256 \times 256$.

Dependences $K(r)$ for other reference reference image $A(x, y)$ sizes had a similar shape. Experimental dependences *3* and *4* for response $A^R(x, y)$ (i.e., the reference image that was dominant during recording) are shown for illustrative purposes and were not approximated.

Figure 5 presents the examples of responses of sub-holograms H^{B2} (2.1) and H^{A2} (2.2) for $r = 1$ and $r = 31$ with the input field shown in Fig. 2, a and the reference images from the input pattern in Fig. 2, b (it bears reminding that reference images are presented separately and sequentially (each for its own superimposed hologram) when superimposed holograms are recorded). For visual

clarity, all the patterns (Figs. 2 and 5) were normalized within the dynamic range of $[0, 255]$ in conversion to the bmp format.

Conclusion

Thus, the responses of sub-holograms forming independently during the development of a multiplex Fourier hologram made up of superimposed holograms, which are recorded sequentially in the $4f$ scheme with angular multiplication of reference beams with a plane wave front on a holographic recording medium with quadratic nonlinearity of the exposure characteristic, are characterized by a model of correlation image restoration. Viewed this way, the model represents hetero-associative memory and may be associated with the concept of ghost imaging (with a number of differences and specific features that are significant both at the conceptual level and in terms of its hardware implementation, which includes digital implementation).

(1) Just as the ghost imaging method, the presented model relies on correlation of two patterns. However, unlike the classical approach of ghost imaging, the model does not require mutual correlation of signal and reference patterns, since restoration of the signal pattern is provided by the autocorrelation component of the correlation function of the input pattern and the reference reference image.

(2) A connection between signal and reference patterns arises as a result of nonlinear processing of the sum of superimposed holograms (1); physically, this is a diffraction grating that emerges when the latent image of a multiplex hologram is revealed. Therefore, for the model to be implemented using digital holography methods, one needs to introduce a separate stage simulating the nonlinear development of the latent image as sum (1) of all superimposed holograms into the calculation algorithm.

(3) A connection between two independent patterns is formed by nonlinear processing of the sum of superimposed holograms in any holographic scheme [23]. However, the correlation mechanism of pattern restoration is characteristic exactly of the $4f$ Fourier holography scheme, since the correlation function in it is (not only a physically real field of amplitudes in the 1st order of diffraction of each superimposed hologram, but also the function included in analytical descriptions (3.1) and (3.2) of the responses of quadratic sub-holograms) is constructed by means of two successive Fourier transforms. Multiplex holograms recorded using other holographic schemes (Fresnel, focused images, lensless Fourier holography, *etc.*) will also generate responses, but these responses are characterized by other models that warrant separate study.

In practical terms, it is important for a number of applications, such as remote sensing and cryptography, that, owing to the correlation mechanism of restoration, both reference images may be realizations of the same homogeneous random field (i.e., have the same variances (average absolute amplitudes)). Therefore, when a message is transmitted, they will not stand out visually from the surrounding background neither in amplitude (intensity) nor in structure (see Fig. 2, *a*). An essential feature of the examined model is the inversion of specific weights of the restored patterns relative to the reference image ones in the responses of sub-holograms: the amplitude of the weaker (by the scalar product criterion) reference image is amplified in the response, while the amplitude of the dominant one is suppressed. This phenomenon may be of practical interest in the context of detection and imaging of small-sized objects against complex structure-like backgrounds.

Conflict of interest

The author declares that he has no conflict of interest.

References

[1] A.V. Lugt. IEEE Trans. Inf. Theory, **10**(2), 139-145 (1964). DOI: 10.1109/TIT.1964.1053650
[2] Psaltis D., Farhat N. Opt. Lett., **10**(2), 98–100 (1985). DOI: 10.1364/OL.10.000098
[3] A.V. Pavlov. Opt. Spectrosc., **98** (6), 949-953 (2005). DOI: 10.1134/1.1953992
[4] D.N. Klyshko. Sov. Phys. Usp., **31**(1), 74-85. (1988). DOI: 10.1070/PU1988v031n01ABEH002537.
[5] D.N. Klyshko. JETP, **94**(6), 82-90 (1988). http://jetp.ras.ru/cgi-bin/dn/e_067_06_1131.pdf.
[6] D.V. Strekalov, A.V. Sergienko, D.N. Klyshko, Y.H. Shih. Phys. Rev. Lett., **74** (18), 3600 (1995). DOI: 10.1103/PhysRevLett.74.3600
[7] D.N. Klyshko. JETP Lett., **6**(1), 23–25 (1967). http://www.jetpletters.ru/ps/1655/article_25244.pdf].
[8] T.B. Pittman, Y.H. Shih, D.V. Strekalov, A.V. Sergienko. Phys. Rev. A, **52** (5), R3429(R) (1995). DOI: 10.1103/PhysRevA.52.R3429
[9] R.S. Bennik, S.J. Bently, R.W. Boyd, J.C. Howell. Phys. Rev. Lett., **92**(3), 033601 (2004). DOI: 10.1103/PhysRevLett.92.033601
[10] A. Gatti, E. Brambilla, M. Bache, L.A. Lugiato. Phys. Rev. Lett., **93**(9), 093602 (2004) DOI: 10.1103/PhysRevLett.93.093602
[11] A. Gatti, E. Brambilla, M. Bache, L.A. Lugiato Phys. Rev. A, **70**(1), 013802 (2004). DOI: 10.1103/PhysRevA.70.013802
[12] D.A. Balakin, D.P. Agapov, P.P. Gostev, S.A. Magnitskii, D.N. Frolovtsev, A.S. Chirkin J. Experimental and Theor. Phys., **135**(6), 779–788 (2022). DOI: 10.1134/S1063776122120159.
[13] D.P. Agapov, I.V. Belovolov, S.A. Magnitskii, D.N. Frolovtsev, A.S. Chirkin J. Experimental Theoretical Phys., **137**(5), 622–629 (2023). DOI: 10.1134/S1063776123110122.
[14] A.V. Belinsky, P.P. Gostev, S.A. Magnitskiy, A.S. Chirkin. JETP Lett., **117**(3), 202–206 (2023). DOI: 10.1134/S0021364022602718.
[15] H. Kellock, T. Setälä, A.T. Friberg, et al. J. Opt., **16**(5), 055702 (2014). DOI: 10.1088/2040-8978/16/5/055702
[16] V.S. Shumigai, P.E. Moreva, B.A. Nasedkin, A.O. Ismagilov, A.V. Chernykh, A.A. Gaidash, A.V. Kozubov, A.D. Kiselev, A.N. Tcypkin J. Optical Technol., **94**(5), 305-309. (2024). DOI: 10.1364/JOT.91.000305.

[17] X. Li, C. Deng, M. Chen, et al. Photonics Research. **3**(4), 153–157 (2015). DOI: 10.1364/PRJ.3.000153
[18] J. Wu, Z. Xie, Z. Liu, et al. Opt. Commun., **359**, 38–43 (2016). DOI: 10.1016/j.optcom.2015.09.039
[19] S. Yuan, L. Wang, X. Liu, X. Zhou. Opt. Lett., **45** (14), 3917–3920 (2020). DOI: 10.1364/OL.392424
[20] Z. Leihong, Z. Zhisheng, Ye Hualong, K. Yi, W. Zhaorui, W. Kaimin, Z. Dawei. Appl. Phys. B, **126**, 136 (2020). DOI: 10.1007/s00340-020-07487-4
[21] R.V. Vinu,, Z. Chen, R. Kumar Singh, Ji-X. Pu. Optica, **7**(12), 1697 (2020). DOI: 10.1364/OPTICA.409886
[22] Vinu Raveendran Pillai Vasantha Kumari, Z. Chen, R. Kumar Singh, J. Pu. Ch. 2 In: *Holography: Recent Advantages and Applications*. Ed. by J. Rosen. (2023). DOI: 10.5772/intechopen.107011
[23] V.V. Orlov. Pis'ma Zh. Tekh. Fiz., **30**(24), 77–81 (2004). https://journals.ioffe.ru/articles/viewPDF/13252 [V.V. Orlov. Technical Physics Lett., **30**(12), 1054-1056 (2004). DOI: 10.1134/1.1846856].
[24] S.A. Kozlov, V.V. Samartsev. *Fundamentals of femtosecond optics* (Elsevier, Washington, 2013), 253 P. DOI: 10.1533/9781782421290
[25] A.V. Pavlov, V.V. Orlov. Quantum Electronics, **49**(3), 246–52 (2019). DOI: 10.1070/QEL16748.
[26] A.M. Kuleshov, E.I. Shubnikov, S.A. Smaeva. Opt. Spectrosc., **60** (6), 791 (1986).
[27] S.A. Aleksandrina, A.M. Kuleshov. Opt. Spectrosc., **68** (3) 381 (1990).
[28] E.I. Shubnikov. Opt. Spectrosc., **62** (2), 268 (1987).
[29] Yu.N. Denisyuk, I.N. Davydova. Opt. Spectrosc., **60** (2), 365 (1986).

Translated by D.Safin